PHYSICAL REVIEW D **83,** 026004 (2011)

Photoemission rate of strongly interacting quark-gluon plasma at finite density

Kwanghyun Jo* and Sang-Jin Sin†

Department of Physics, Hanyang University, Seoul 133-791, Korea

(Received 14 June 2010; published 12 January 2011)

We calculate the thermal spectral function of strongly interacting Yang-Mills plasma with finite density using the holographic technique. The gravity dual of the finite temperature and density is taken as the Reissner-Nordström–anti-de Sitter black hole. In the presence of charge, linearized vector modes of gravitational and electromagnetic perturbation are coupled with each other. By introducing master variables for these modes, we solve the coupled system and calculate spectral function. The spectral function gets a new peak due to the density effect, which is most dramatic in the momentum plot with fixed frequency. We also calculate the photoemission rate of our gauge theory plasma from the spectral function for lightlike momentum. AC, dc conductivity, and their density dependence is also computed.

DOI: 10.1103/PhysRevD.83.026004 PACS numbers: 11.25.Tq, 12.38.Mh

I. INTRODUCTION

The gauge/gravity duality [1–3] opened a new possibility to quantitative study for strongly interacting systems. Although it is not developed enough to describe realistic QCD, we expect to learn some features of QCD from it based on the universality of the hydrodynamics: in the long wavelength limit, the details of the theory do not matter. For example, the shear viscosity/entropy ratio [4,5] η/s is universal if we neglect the higher derivative terms. We also expect, due to analytic structure of the theories, that there are similarities of supersymmetric and nonsupersymmetric theories which can continue to the finite wavelength/frequency regime.

The quarks and gluons are liberated at high enough temperature. However, over $T_c < T < 2 \sim 3T_c$, the experimental data shows that quarks and gluons are not free but are strongly interacting: the small viscosity and the presence of the coherent flow show that the interactions should be very strong. Such strongness of the interaction is the motivation why one has to abandon perturbative QCD in such an energy/temperature regime. One way to avoid that difficulty is to rely on holographic QCD (hQCD) for the quark-gluon plasma in the Relativistic Heavy Ion Collider (RHIC). The hydrodynamic calculations of hQCD were shown to be useful to discuss the transport phenomena [6,7]. It is interesting to see what happens in the Large Hadron Collider (LHC) where the energy scale is much higher [8].

The finite density effect is a very essential ingredient to understand how the core of the neutron star and the early universe behave. It may uncover some significant features of the evolution of our universe, galaxies, and stars. At the RHIC experiment, the temperature reached is above T_c but the density is almost zero. In the near future the Japan Proton Accelerator Research Complex, LHC, and especially the Facility for Antiproton and Ion Research, which probes the regime of a few times of normal nuclear density [9], will tell us much about the density effect of quarks and gluons. The holographic study for the system with finite density in the hydrodynamic regime was made in [10–14].

The dual gravity background for the finite density and temperature is taken to be Reissner-Nordström–AdS (RN-AdS) black hole. The bulk U(1) charge is usually identified with the U(1) R charge rather than the particle number density of the boundary field theory. Here we work out this case and hope that baryon charge density is similar in its effect. In the phase diagram, we know much about the high temperature, low density regime but not the low temperature high density regime. Previously we studied some issues like meson mass shifted by density effect for zero temperature, finite density sector [15]. Now we will study the effect of both finite temperature and density. The bulk U(1) charge is identified with the particle number density of the boundary field theory. To see the finite frequency/momentum dependence of the response of the system, the spectral function is a good tool. It gives us ac conductivity and its trace is related to the photoemission and dilepton production rate [16–18].

The spectral function with and without medium density in the probe brane approach was already calculated [19–26]. However, in that approach the gravity backreaction to the presence of the charge is neglected. In this paper, we take a bottom-up approach where the backreaction is taken into account. We will compute the spectral function of tensor and vector modes which describe the fluctuation of energy momentum tensor and currents of hot plasma. After that the finite temperature and density effects of photoemission rate are calculated and discussed.

The most notable effect of the density is the appearance of the new peak in the spectral function which is absent at zero chemical potential. This is especially dramatic in the momentum plot of the spectral function as we shall see later. We attribute the origin of this effect to the appearance of the diffusion pole which was discovered in [13]. Since

*jokh38@gmail.com
†sjsin@hanyang.ac.kr

the residue of the pole is proportional to the charge, we can expect that the new peak in spectral density is enhanced as charge increases. Indeed the numerical calculation confirms such expectations.

II. A RECIPE FOR GREEN'S FUNCTION

In this section, we will briefly review how to calculate the thermal spectral function. To describe thermalized plasma holographically we need the black hole background. The general equations of motion for the linearized fluctuations in this background are

$$E''_\alpha(u) + P(\mathfrak{w}, \mathfrak{q}, u)E'_\alpha(u) + Q(\mathfrak{w}, \mathfrak{q}, u)E_\alpha(u) = 0, \quad (2.1)$$

where E_α denote the fluctuating fields in a given background and α runs 1 to n, the number of independent fields, and $\mathfrak{w}$, $\mathfrak{q}$ are dimensionless frequency and momentum. Near the boundary ($u \sim 0$)[1] there are two local Frobenius solutions Φ_1, Φ_2:

$$\Phi_1 = u^{\Delta_-}(1 + \cdots) \qquad \Phi_2 = u^{\Delta_+}(1 + \cdots). \quad (2.2)$$

$\Delta_\pm$ is the solution of the indicial equation near the boundary, $\Delta_+ > \Delta_-$ where Δ_+ is the conformal dimension of an operator, and Δ_- is the dimension of the dual source field. Near the horizon, $u = 1$, there are also two local solutions:

$$\begin{aligned} \phi_1 &= (1-u)^{-i\mathfrak{w}/2}(1 + \cdots) \\ \phi_2 &= (1-u)^{i\mathfrak{w}/2}(1 + \cdots). \end{aligned} \quad (2.3)$$

The two different local solutions of Eq. (2.1) should be matched:

$$\begin{aligned} E_\alpha &= \mathcal{A}(\mathfrak{w}, \mathfrak{q})\Phi_1 + \mathcal{B}(\mathfrak{w}, \mathfrak{q})\Phi_2 \\ &= \mathcal{C}(\mathfrak{w}, \mathfrak{q})\phi_1 + \mathcal{D}(\mathfrak{w}, \mathfrak{q})\phi_2. \end{aligned} \quad (2.4)$$

However, not all solutions are allowed physically because this system contains the black hole: no outgoing wave can propagate from the horizon, therefore we should impose $\mathcal{D} = 0$, which is called the infalling boundary condition. Taking the normalization $\mathcal{C} = 1$ using the linearity of differential equation, we have

$$\phi_1(u) = \mathcal{A}(\mathfrak{w}, \mathfrak{q})\Phi_1(u) + \mathcal{B}(\mathfrak{w}, \mathfrak{q})\Phi_2(u). \quad (2.5)$$

Note that the coefficient $\mathcal{A}$ is the source of the boundary theory operator $\mathcal{A}(\mathfrak{w}, \mathfrak{q}) = J_\alpha(\mathfrak{w}, \mathfrak{q})$, so by differentiating the generating functional twice with respect to J_α we get the retarded Green function. Another coefficient $\mathcal{B}$ corresponds to the condensate or vacuum expectation value of the operator $\mathcal{O}_\alpha$ which couples to the source J_α. The retarded Green function is given by the ratio between $\mathcal{A}$, $\mathcal{B}$. We will give a sketch of the on-shell quadratic action, with Eqs. (2.2) and (2.5):

[1]Our coordinate u covers the range $0 \le u \le 1$ where 0 is the position of the boundary and 1 is the position of the horizon.

$$\begin{aligned} &S_{\text{on-shell}} \\ &\sim \int d^{d+1}x\sqrt{g}E^{\alpha\prime}E'_\alpha \sim \int d^dx\Big[u^{-(\Delta_+ + \Delta_- - 1)}\mathcal{A}^2 \\ &\quad \times \Big(u^{\Delta_-} + \frac{\mathcal{B}}{\mathcal{A}}u^{\Delta_+}\Big)\Big(\Delta_- u^{\Delta_- - 1} + \Delta_+ \frac{\mathcal{B}}{\mathcal{A}}u^{\Delta_+ - 1}\Big)\Big]_{u\to 0} \\ &\sim \int d^dx\mathcal{A}^2\Big[u^{-(\Delta_+ + \Delta_- - 1)}(\Delta_- u^{2\Delta_- - 1} \\ &\quad + (\Delta_+ + \Delta_-)\frac{\mathcal{B}}{\mathcal{A}}u^{\Delta_+ + \Delta_- - 1}\Big)\Big]_{u\to 0} \\ &\sim \int d^dx\mathcal{A}^2\Big[\Delta_- u^{\Delta_- - \Delta_+} + (\Delta_+ + \Delta_-)\frac{\mathcal{B}}{\mathcal{A}}\Big]_{u\to 0}. \end{aligned} \quad (2.6)$$

Obviously $u^{\Delta_- - \Delta_+}$ is divergent ($\Delta_- < \Delta_+$) so it should be renormalized holographically [27] or we can ignore it because the imaginary part of the Green's function does not care about the real number which comes from the first term. For the issues on how to regulate the on-shell action, see Appendix D. The spectral function is its imaginary part [20]. Notice that

$$\begin{aligned} &\frac{\mathcal{B}}{\mathcal{A}} = \frac{1}{\Phi_2(u)}\Big(\frac{\phi_1(u)}{\phi_1(0)} - \Phi_1(u)\Big) \\ &\chi = \mathrm{Im}G^{\text{ret}} = \mathrm{Im}\frac{\mathcal{B}}{\mathcal{A}} = \frac{1}{\Phi_2}\mathrm{Im}\Big(\frac{\phi_1(u)}{\phi_1(0)}\Big), \\ &\qquad \text{where } \mathcal{A} = \lim_{u\to 0}\frac{\phi_1(u)}{u^{\Delta_-}}. \end{aligned} \quad (2.7)$$

Here Φ_i is real because the equation of motion and initial conditions are real for Φ_i. The above expression is independent of u since it is a kind of conserved flux [6],

$$S_{\text{bdry}}[\phi_0] = \int \frac{d^4k}{(2\pi)^4}\phi_0(-k)\mathcal{G}(k, u)\phi_0(k)|_{u=0}^{u=1}, \quad (2.8)$$

where $\mathcal{G} = \mathcal{N}\frac{\mathcal{B}}{\mathcal{A}}$, with $\mathcal{N}$ the normalization constant. The retarded Green function is defined by the recipe [6]

$$\begin{aligned} G^R_{ij}(K) &= -2\mathcal{G}_{ij}(K, u = 0) \quad i = j \\ &= -\mathcal{G}_{ij}(K, u = 0) \quad i \neq j. \end{aligned} \quad (2.9)$$

From Eq. (2.7), the only thing we should know is the value of $\phi_1(u)$, $\Phi_2(u)$. The spectral function, for example, is given when $\Delta_- = 0$:

$$\chi_{ii} = -2\mathcal{N}\lim_{u\to .5}\Big[\frac{1}{\Phi_2(u)}\mathrm{Im}\Big(\frac{\phi_1(u)}{\phi_1(u = 0)}\Big)\Big]. \quad (2.10)$$

Given the normalization constant $\mathcal{N}$ we can calculate the spectral function numerically.

III. RN ADS

The dual geometry for the finite temperature and density is chosen as a charged AdS black hole [14]. The action is

$$S = \frac{1}{2G_5^2}\int d^5x\sqrt{-g}(\mathcal{R} - 2\Lambda) + \frac{1}{4g_5^2}\int d^5x\sqrt{-g}F^2 + \frac{1}{G_5^2}\int d^4x\sqrt{-g^{(4)}}K, \tag{3.1}$$

where the cosmological constant is $\Lambda = -\frac{(d-1)(d-2)}{2l^2}$, the last term is the Gibbons-Hawking term, K is the extrinsic curvature on the boundary, and l is the AdS radius. The metric of RN AdS is

$$ds^2 = \frac{r^2}{l^2}(-f(r)dt^2 + d\vec{x}^2) + \frac{l^2}{r^2 f(r)}dr^2$$
$$f(r) = 1 - \frac{ml^2}{r^4} + \frac{q^2l^2}{r^6}, \tag{3.2}$$
$$A_t = -\frac{Q}{r^2} + \mu,$$

where the gauge charge Q is related to the black hole charge q,

$$g_5^2 = \frac{2Q^2}{3q^2}G_5^2, \qquad Q^2 = \frac{3g_5^2}{2G_5^2}q^2, \tag{3.3}$$

the five-dimensional gauge theory coupling constant g_5 and the gravitational constant G_5[2] can be chosen as [28]

$$\frac{l}{g_5^2} = \frac{N_c N_f}{4\pi^2}, \qquad \frac{l^3}{G_5^2} = \frac{N_c^2}{4\pi^2} \tag{3.4}$$

but we will not use these parameters explicitly. The metric function $f(r)$ is rewritten as

$$f(r) = \frac{1}{r^6}(r^2 - r_+^2)(r^2 - r_-^2)(r^2 - r_0^2),$$
$$r_\alpha^{-2} = \frac{m}{3q^2}\left(1 + 2\cos\left(\frac{\theta}{3} + \varphi_\alpha\right)\right), \tag{3.5}$$

where $\alpha = +, -, 0$ and $\varphi_+ = 4\pi/3$, $\varphi_- = 0$, $\varphi_0 = 2\pi/3$. The charge is expressed by θ and m,

$$q^4 = \frac{4m^3l^2}{27}\sin^2\left(\frac{\theta}{2}\right),$$
$$\theta = \arctan\left(\frac{3\sqrt{3}q^2\sqrt{4m^3l^2 - 27q^4}}{2m^3l^2 - 27q^4}\right). \tag{3.6}$$

Finally, the black hole temperature is given as

$$T = \frac{r_+^2 f'(r_+)}{4\pi l^2} = \frac{r_+}{\pi l^2}\left(1 - \frac{q^2l^2}{2r_+^6}\right) \equiv \frac{1}{2\pi b}\left(1 - \frac{a}{2}\right), \tag{3.7}$$

where a, b are

$$a \equiv \frac{q^2l^2}{r_+^6}, \qquad b \equiv \frac{l^2}{2r_+}. \tag{3.8}$$

From the horizon regularity, the black hole charge q is related with the chemical potential μ,

$$\mu = \frac{4Qb^2}{l^4} = \frac{1}{2b}\frac{g_5 l}{G_5}\sqrt{\frac{3a}{2}},$$
$$a = \frac{3 + 2\bar{\mu}^2 - \sqrt{9 + 12\bar{\mu}^2}}{\bar{\mu}^2}, \qquad \text{where } \bar{\mu} = \frac{\mu}{T}\frac{G_5}{\pi g_5 l}. \tag{3.9}$$

Notice that there is maximum value of q, $q^4 \le \frac{4}{27}m^3l^2$ which corresponds to $a = 2$. Horizon radius r_+ should be real, so $1 + 2\cos(\theta/3 + 4\pi/3)$ must be positive.

It is very useful to express the frequency and momentum as dimensionless quantities $\mathfrak{w} = w/(2\pi T)$, $\mathfrak{q} = k/(2\pi T)$. This choice is good enough to see the finite temperature behavior of the system but not good in the zero temperature limit. An alternative way is to rescale w and k by the black hole radius r_+, that is by b: let $\tilde{\mathfrak{w}} = bw$, $\tilde{\mathfrak{q}} = bk$. At the extremal limit, by Eq. (3.6), $4m^3l^2 = 27q^4$ and $\theta = \pi$,

$$r_+ = \left(\frac{l^2}{2}\right)^{1/6}q^{1/3}, \qquad a = 2, \qquad b = \left(\frac{l^2}{2}\right)^{5/6}q^{-1/3} \tag{3.10}$$

and the chemical potential is written

$$\mu = \frac{\sqrt{3}}{2}\frac{el}{G_5}\frac{1}{b}. \tag{3.11}$$

If we rescale w and k with b, in the extremal limit we rescale w and k with chemical potential, $\tilde{\mathfrak{w}} \sim w/\mu$, $\tilde{\mathfrak{q}} \sim k/\mu$.

The origin of the charged black hole in string theory can be understood by the STU [29] model: the diagonally charged STU black hole is RN AdS. The diagonal U(1) is the subgroup of the SU(4) R symmetry originally but here we assume that this U(1) is a part of the flavor U(1) group which is relevant if we assume that the bulk filling branes [28] are embedded in our AdS_5 space time.[3] The merit of doing this is that we can have a backreacted gravitational background which is a solution of the glue-quark coupled system. In terms of gauge theory, it means that our approach is beyond quenched approximation.

IV. TENSOR MODE

The gravitational and gauge field perturbation is classified by the boundary SO(2) rotational symmetry. This classification is summarized in Appendix A. Tensor mode perturbation is easy to treat because it is completely decouple from other fields. The equation of motion for the h_{xy} component is

$$h_y^{x\prime\prime} + \frac{(r^5 f)'}{r^5 f}h_y^{x\prime} + \frac{l^4}{r^4 f^2}(w^2 - k^2 f)h_y^x = 0, \tag{4.1}$$

[2]Usually the five-dimensional gravitational constant G_5 is used as $\kappa^2 = 8\pi G_5$ but here we will use G_5 as κ itself.

[3]Please note that this is no more than a conceptual introduction of the bottomup approach in string theory.

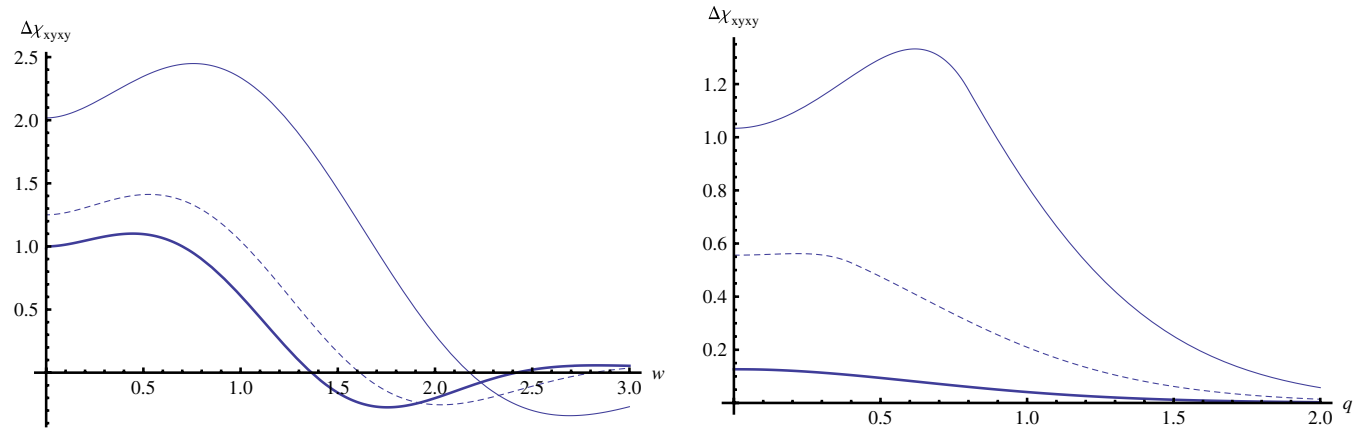

FIG. 1 (color online). The difference of thermal spectral function and zero temperature spectral function of $\Delta\chi_{xy,xy}/\mathfrak{w}$. Left: with fixed $\mathfrak{q}=0$ when $\bar{\mu}=0$ (thick), 0.5 (dashed), 1 (thin); right: $\Delta\chi_{xy,xy}$ vs $\mathfrak{q}$ plot and $w=0.1$(thick), 0.4 (dashed), 0.8 (thin) with fixed $\bar{\mu}=0.5$.

where the prime denotes derivative with respect to r and $h_y^x = g^{(0)xx}h_{xy}$. Introducing new coordinate $u = r_+^2/r^2$,

$$ds^2 = \frac{(\pi T l)^2}{u}(-f(u)dt^2 + d\vec{x}^2) + \frac{l^2}{4u^2 f(u)}du^2, \qquad f(u) = (1-u)(1+u-au^2). \tag{4.2}$$

The equation of motion is simplified

$$h_y^{x\prime\prime} - \frac{f - uf'}{uf}h_y^{x\prime} + \frac{1}{uf^2}(\tilde{\mathfrak{w}}^2 - \tilde{\mathfrak{q}}^2 f)h_y^x = 0, \tag{4.3}$$

where

$$\tilde{\mathfrak{q}} = bk = \frac{k}{2\pi T}\left(1-\frac{a}{2}\right) = \mathfrak{q}\left(1-\frac{a}{2}\right), \qquad \tilde{\mathfrak{w}} = \frac{w}{2\pi T}\left(1-\frac{a}{2}\right) = \mathfrak{w}\left(1-\frac{a}{2}\right). \tag{4.4}$$

This differential equation has two independent solutions near the boundary,

$$h_y^x = \mathcal{A}\Phi_1(u) + \mathcal{B}\Phi_2(u), \tag{4.5}$$

where

$$\Phi_1(u) = 1 + \cdots + h_l \log(u)\Phi_2(u), \qquad \Phi_2(u) = u^2(1+\cdots). \tag{4.6}$$

By choosing $\mathcal{A} = \phi_1(0)$ in Eq. (2.5), we get the normalized solution for tensor mode

$$h_y^x(u) = \frac{\phi_1(u)}{\phi_1(0)} = \Phi_1(u) + \frac{\mathcal{B}}{\mathcal{A}}\Phi_2(u). \tag{4.7}$$

The on-shell action is given in Eq. (5.7) of [13],

$$S[h_y^x] = \frac{l^3}{32G_5^2 b^4}\int \frac{d^4k}{(2\pi)^4}\left(\frac{f(u)}{u}h_y^x(-k,u)h_y^{x\prime}(k,u)\right)\Big|_{u=1}^{u=0}. \tag{4.8}$$

Our normalization is such that $h_y^x(u) \to 1$ at the boundary.[4] By taking the imaginary part of the Green's function and renormalizing divergent terms, the thermal spectral function is

$$\chi(\mathfrak{w},\mathfrak{q})_{xy,xy} = \frac{l^3}{16G_5^2 b^4}\,\mathrm{Im}\left(2\frac{\mathcal{B}}{\mathcal{A}}\right). \tag{4.9}$$

Here the ratio $\mathcal{B}/\mathcal{A}$ is

$$\frac{\mathcal{B}}{\mathcal{A}} = \frac{1}{\Phi_2(u)}\left(\frac{\phi_1(u)}{\phi_1(0)} - \Phi_1(u)\right). \tag{4.10}$$

This ratio is independent of the evaluation point. As explained before, imposing the infalling condition at the horizon and Dirichlet boundary condition at the UV boundary, we get the numerical solution for $\phi_1(u)$ and $\Phi_2(u)$,

$$\chi(w,k)_{xy,xy} = \frac{l^3}{16G_5^2 b^4}\,\mathrm{Im}\left(\frac{2}{\Phi_2(u)}\frac{\phi_1(u)}{\phi_1(0)}\right). \tag{4.11}$$

Using $b = (1-a/2)/2\pi T$, one can show that the zero temperature spectral function is

$$\chi(w,k)_{xy,xy}^{T\to 0} = \frac{(2\pi T)^4 l^3}{16G_5^2}\pi(\mathfrak{w}^2-\mathfrak{q}^2)^2\theta(w^2-k^2). \tag{4.12}$$

See Appendix B for details. Figure 1 shows the difference between the normalized thermal spectral function at nonzero and zero temperatures for $\Delta\chi_{xy,xy}$. The thick line is the zero chemical potential case $\bar{\mu}=0$ which is the AdS Schwarzschild case of Ref. [21]. The dashed and the solid lines correspond to the $\bar{\mu}=0.5, 1$ case, respectively. When the chemical potential μ increases, the spectral difference grows up and the position of the small peak is shifted to the larger $\mathfrak{w}$. The position of the peak in the spectral difference is the pole position of the retarded Green's function [19].

[4]More properly, we should express $h_y^x(u,k) = \hat{h}_y^x(k)h_y^x(u)$, where the hatted variable is the value at the boundary or the external source of the boundary theory.

The shift of the peak is the shift of the quasinormal mode. When chemical potential grows in the unit of T, the pole position grows faster than T.

The right side of Fig. 1 shows the spectral function as a function of spatial momentum $\mathfrak{q}$. When $\mathfrak{w} = 0$, the peak position can be identified with the inverse screening length. However, for the tensor mode, there is no peak for $\mathfrak{w} = 0$. As we know SYM has conformal symmetry, hence it cannot have any scale. For the finite μ, there is a broad peak and the peak is more sharpened when chemical potential grows. This shows that in a dense system the thermal particle collides more often so that the particles propagate shorter distance. For the lightlike momentum, this screening is maximized. For spacelike momentum, the thermal fluctuation of spectral function rapidly vanishes leaving only a zero temperature piece.

V. VECTOR MODE

Vector-type perturbation consists of three independent fields, h_{xt}, h_{xz}, A_x, and equations of motion for these modes are coupled with each other. In the hydrodynamic limit, this mode has a diffusion pole so that it is also named as a diffusive mode. Here we are interested in the general energy/momentum regime. The equations of motion for vector modes are

$$\begin{aligned}
0 &= h_t^{x\prime\prime} - \frac{1}{u}h_t^{x\prime} - \frac{(1-\frac{a}{2})^2}{uf}(\mathfrak{w}\mathfrak{q}h_z^x + \mathfrak{q}^2 h_t^x) - 3auB' \\
0 &= \mathfrak{q}f h_z^{x\prime} + \mathfrak{w}h_t^{x\prime} - 3a\mathfrak{w}uB \\
0 &= h_z^{x\prime\prime} + \frac{(f/u)'}{f/u}h_z^{x\prime} + \frac{(1-\frac{a}{2})^2}{uf^2}(\mathfrak{w}^2 h_z^x + \mathfrak{w}\mathfrak{q}h_t^x) \\
0 &= B'' + \frac{f'}{f}B' + \frac{(1-\frac{a}{2})^2}{uf^2}(\mathfrak{w}^2 - \mathfrak{q}^2 f)B - \frac{h_t^{x\prime}}{f}.
\end{aligned} \tag{5.1}$$

This equation is simplified by introducing a gauge invariant combination $Z_1 = \mathfrak{w}h_z^x + \mathfrak{q}h_t^x$,[5]

$$\begin{aligned}
0 &= Z_1'' + \left(\frac{f'\tilde{\mathfrak{w}}^2}{f(\tilde{\mathfrak{w}}^2 - \tilde{\mathfrak{q}}^2 f)} - \frac{1}{u}\right)Z_1' + \frac{(\tilde{\mathfrak{w}}^2 - \tilde{\mathfrak{q}}^2 f)}{uf^2}Z_1 \\
&\quad - 3au\tilde{\mathfrak{q}}\left(B' + \frac{\tilde{\mathfrak{w}}^2 f'}{f(\tilde{\mathfrak{w}}^2 - \tilde{\mathfrak{q}}^2 f)}B\right) \\
0 &= B'' + \frac{f'}{f}B' + \left[\frac{\tilde{\mathfrak{w}}^2 - \tilde{\mathfrak{q}}^2 f}{uf^2} - \frac{3au}{f} - \frac{3au\tilde{\mathfrak{q}}^2}{\tilde{\mathfrak{w}}^2 - \tilde{\mathfrak{q}}^2 f}\right]B \\
&\quad + \frac{\tilde{\mathfrak{q}}}{(\tilde{\mathfrak{w}}^2 - \tilde{\mathfrak{q}}^2 f)}Z_1',
\end{aligned} \tag{5.2}$$

[5]We can always choose a certain gauge to eliminate some components of gravitational and electromagnetic perturbation. But by choosing these gauge invariant combinations, we have at least two merits: first we study this system in a gauge independent way; second, to make the gauge invariant combination we use all of the constraint so we do not worry about the consistency of our equations of motion and their solutions.

where $\tilde{\mathfrak{w}} = (1 - \frac{a}{2})\mathfrak{w}$. It is not easy to solve these 2nd order coupled differential equations, but the authors of [13] have decoupled these equations by introducing master variables. Let us define first $\Psi_\pm$ as

$$\Psi_\pm = -\frac{f\tilde{\mathfrak{q}}}{\tilde{\mathfrak{w}}^2 - \tilde{\mathfrak{q}}^2 f}Z_1' + \left(-3au\frac{f\tilde{\mathfrak{q}}^2}{\tilde{\mathfrak{w}}^2 - \tilde{\mathfrak{q}}^2 f} + C_\pm\right)B. \tag{5.3}$$

The equation of motion is rewritten as

$$\Psi_\pm'' + \frac{f'}{f}\Psi_\pm' + \left(\frac{\tilde{\mathfrak{w}}^2 - \tilde{\mathfrak{q}}^2 f}{uf^2} - \frac{f'}{uf} - \frac{C_\pm}{f}\right)\Psi_\pm = 0, \tag{5.4}$$

where $C_\pm$ is

$$\begin{aligned}
C_\pm &= (1+a) \pm \sqrt{(1+a)^2 + 3ab^2k^2} \\
&= (1+a) \pm \sqrt{(1+a)^2 + 3a\left(1 - \frac{a}{2}\right)^2\mathfrak{q}^2} \\
&= (1+a)(1 \pm \gamma), \qquad \text{where } \gamma = \sqrt{1 + \frac{3a}{4}\left(\frac{2-a}{1+a}\right)^2\mathfrak{q}^2}.
\end{aligned} \tag{5.5}$$

In order to use our recipe for spectral function, we need the on-shell action for vector modes:

$$\begin{aligned}
S_{os} &= \frac{l^3}{32G_5^2 b^4}\int\frac{d^4k}{(2\pi)^4} \\
&\quad \times \left(\frac{1}{u}h_t^x(-k,u)h_t^{x\prime}(k,u) - \frac{f(u)}{u}h_z^x(-k,u)h_z^{x\prime}(k,u)\right. \\
&\quad \left. - 3af(u)B(-k,u)B'(k,u)\right)\Big|_{u=0}^{u=1} \\
&= \frac{l^3}{32G_5^2 b^4}\int\frac{d^4k}{(2\pi)^4}\left(\frac{1}{u}\frac{f}{\tilde{\mathfrak{w}}^2 - \tilde{\mathfrak{q}}^2 f}Z_1 Z_1' - 3afBB'\right. \\
&\quad \left. + \frac{\tilde{\mathfrak{w}}^2}{\tilde{\mathfrak{w}}^2 - \tilde{\mathfrak{q}}^2 f}3auBh_t\right).
\end{aligned} \tag{5.6}$$

From the equations for master field, we can get the spectral function of master fields. We however need the spectral function of original variables not the master field itself. In Ref. [30], the authors showed a systematic way to compute the spectral function of original variables in terms of master variables. Let us first find the series solution of Z_1, B,

$$\begin{aligned}
Z_1 &= \hat{Z}_1(1 + (\tilde{\mathfrak{w}}^2 - \tilde{\mathfrak{q}}^2)u + \cdots) + \frac{\pi_Z}{2}u^2 + \cdots \\
B &= \hat{B}(1 + \cdots) + \pi_B u + \cdots,
\end{aligned}$$

which defines the conjugate momentums π_Z, π_B. The boundary action can be written in terms of the boundary values of original variables and their conjugate momentums:

$$S_{bd} = \frac{l^3}{32G_5^2 b^4}\int\frac{d^4k}{(2\pi)^4}\left(\frac{\hat{Z}_1\pi_Z}{\tilde{\mathfrak{w}}^2 - \tilde{\mathfrak{q}}^2} - 3a\hat{B}\pi_B + \cdots\right), \tag{5.7}$$

where $\hat{Z}_1$, $\hat{B}$ are the boundary values of the fields and π_Z, π_B are their conjugate momentum which will be identified with one point function, and dots denote contact terms which do not have any derivatives with respect to u. Note that these conjugate momentums depend on the boundary source terms implicitly. The master variables $\Psi_{\pm 1}$ and $\Psi_{\pm 2}$ have series solutions near the boundary,

$$\Psi_\pm = \hat{\Psi}_\pm(1 + \cdots + \hat{\Pi}_\pm u + \cdots).$$

Define the transformation matrix R,

$$\mathrm{R} = \begin{pmatrix} -\frac{\tilde{\mathfrak{q}}}{\tilde{\mathfrak{w}}^2 - \tilde{\mathfrak{q}}^2} & C_+ \\ -\frac{\tilde{\mathfrak{q}}}{\tilde{\mathfrak{w}}^2 - \tilde{\mathfrak{q}}^2} & C_- \end{pmatrix}, \tag{5.8}$$

the boundary value of the master fields is simply related to the boundary value of the original fields by R,

$$\begin{aligned} \begin{pmatrix} \Psi_+ \\ \Psi_- \end{pmatrix} &= \mathrm{R} \begin{pmatrix} (Z_1)'(u=0) \\ \hat{B} \end{pmatrix} \\ &= \mathrm{R} \begin{pmatrix} (\tilde{\mathfrak{w}}^2 - \tilde{\mathfrak{q}}^2)\hat{Z}_1 \\ \hat{B} \end{pmatrix} \begin{pmatrix} \Psi_+ \Pi_+ \\ \Psi_- \Pi_- \end{pmatrix} = \mathrm{R} \begin{pmatrix} \pi_Z \\ \pi_B \end{pmatrix}. \end{aligned} \tag{5.9}$$

Then the conjugate momenta π_Z, π_B are written as

$$\begin{pmatrix} \pi_Z \\ \pi_B \end{pmatrix} = \mathrm{R}^{-1}\,\mathrm{Diag}(\Psi_+, \Psi_-) \begin{pmatrix} \Pi_+ \\ \Pi_- \end{pmatrix}. \tag{5.10}$$

The boundary action is now written only by boundary values $(\hat{Z}_1, \hat{B})$ and conjugate momentum of master field $\Pi_\pm$. The two point function for h_t^x and h_z^x is related to the gauge invariant variable Z_1 as

$$\begin{aligned} \mathcal{G}_{xtxt} &= \frac{\delta^2 S_{bd}}{\delta \hat{h}_t^x \delta \hat{h}_t^x} = \left(\frac{\delta \hat{Z}_1}{\delta h_t^x}\right)^2 \frac{\delta^2 S_{bd}}{\delta \hat{Z}_1 \delta \hat{Z}_1} = \tilde{q}^2 \frac{\delta^2 S_{bd}}{\delta \hat{Z}_1 \delta \hat{Z}_1}, \\ \mathcal{G}_{xx} &= \left(\frac{\delta \hat{B}}{\delta \hat{A}_x}\right)^2 \frac{\delta^2 S_{bd}}{\delta \hat{B} \delta \hat{B}} = \frac{1}{\mu^2} \frac{\delta^2 S_{bd}}{\delta \hat{B} \delta \hat{B}}. \end{aligned} \tag{5.11}$$

Therefore the correlation functions are

$$\begin{aligned} \mathcal{G}_{xt,xt} &= \frac{l^3}{32 G_5^2 b^4} \tilde{\mathfrak{q}}^2 \frac{C_- \hat{\Pi}_+ - C_+ \hat{\Pi}_-}{C_+ - C_-}, \\ \mathcal{G}_{xz,xz} &= \frac{\mathfrak{w}^2}{\mathfrak{q}^2} \mathcal{G}_{xt,xt} \\ \mathcal{G}_{xt,x} &= \mathcal{G}_{x,xt} = \tilde{\mathfrak{q}}^2 \frac{l^2 \sqrt{6a}}{32 G_5 e b^3} \frac{\hat{\Pi}_+ - \hat{\Pi}_-}{C_+ - C_-} \\ \mathcal{G}_{x,x} &= \frac{l}{4e^2 b^2} \frac{C_+ \hat{\Pi}_+ - C_- \hat{\Pi}_-}{C_+ - C_-} \\ &= \frac{l}{4e^2 b^2} \frac{1}{2} \left(\frac{\hat{\Pi}_+ - \hat{\Pi}_-}{\gamma} + \hat{\Pi}_+ + \hat{\Pi}_- \right). \end{aligned} \tag{5.12}$$

Note that when spatial momentum $\mathfrak{q}$ or density "a" vanishes two point function $\mathcal{G}_{xt,x}$ vanishes. It means that the holographic operator mixing between Z_1 and A_x comes from the density effects. By following the standard recipe described in Sec. 2.II, $\Pi_\pm$, the conjugate momentum of master fields, are computed as the ratio of two connection coefficients,

$$\begin{aligned} \Psi_\pm &= \mathcal{A}_\pm(1 + \cdots) + \mathcal{B}_\pm u(1 + \cdots) \\ &= \hat{\Psi}_\pm[1 + \cdots + \hat{\Pi}_\pm u \cdots]. \end{aligned} \tag{5.13}$$

By comparing Eq. (5.13) with Eq. (2.5) we get the conjugate momentum of the master fields as a ratio of connection coefficient of near boundary solutions of them,

$$\mathrm{Im}\,\frac{\mathcal{B}_\pm}{\mathcal{A}_\pm} = \mathrm{Im}\hat{\Pi}_\pm. \tag{5.14}$$

By imposing infalling IR boundary condition for $\Psi_\pm$, the spectral functions are computed:

$$\begin{aligned} \chi_{xtxt} &= 2\,\mathrm{Im}\mathcal{G}_{xtxt}, & \chi_{xzxz} &= \frac{\mathfrak{w}^2}{\mathfrak{q}^2}\chi_{xtxt}, \\ \chi_{x,xt} &= \mathrm{Im}\mathcal{G}_{xxt}, & \chi_{xx} &= 2\,\mathrm{Im}\mathcal{G}_{xx}. \end{aligned} \tag{5.15}$$

The spectral function is plotted in terms of $\mathfrak{w}$, $\mathfrak{q}$. Figure 2 shows the imaginary part of the G_{xx} divided by w, which is AC conductivity of thermalized plasma (with normalization constant, $\frac{1}{2}\frac{l}{g_5^2} 2\pi T$). The peak position becomes larger as the charge increases. The strength of that peak also increases, when charge grows. In Ref. [21], they calculate only the zero density case which is denoted by the thick line in Fig. 2. The right part of Fig. 2 is the density dependence of DC conductivity. From the spectral function, DC conductivity can be computed by taking the zero frequency limit, $\sigma_E = \lim_{w\to 0} \frac{\chi_{xx}(w,k=0)}{w}$. As density increases, it decreases and in sufficiently large density regime, DC conductivity is negligible. This is rather surprising since the Drude formula in Maxwell theory says the conductivity is proportional to the density of the charge carrier. It seems that interaction between the charge carriers dominates the abundant effect. Such a drastic reduction of the DC conductivity can be another explanation of the jet quenching phenomena which are different from the explanation in Refs. [31,32]. In a highly dense system, the strongly interacting plasma cannot carry charge over long distances because of density effect. If this is the relevant mechanism, raising the temperature suppresses the jet quenching in LHC since it reduces $\bar{\mu} \sim \mu/T$.

In Fig. 3, we plot the spectral function χ_{xx} in terms of spatial momentum with fixed frequency. The left part shows thick, dashed, and thin lines corresponding to $\mathfrak{w} = 0.1, 0.3, 0.5$ with $\bar{\mu} = 1$ and the right part of Fig. 3 also shows thick, dashed, and thin lines corresponding to $\bar{\mu} = 1, 2, 3$ with $\mathfrak{w} = 0.1$. These results can be interpreted as an inverse thermal screening length of the super

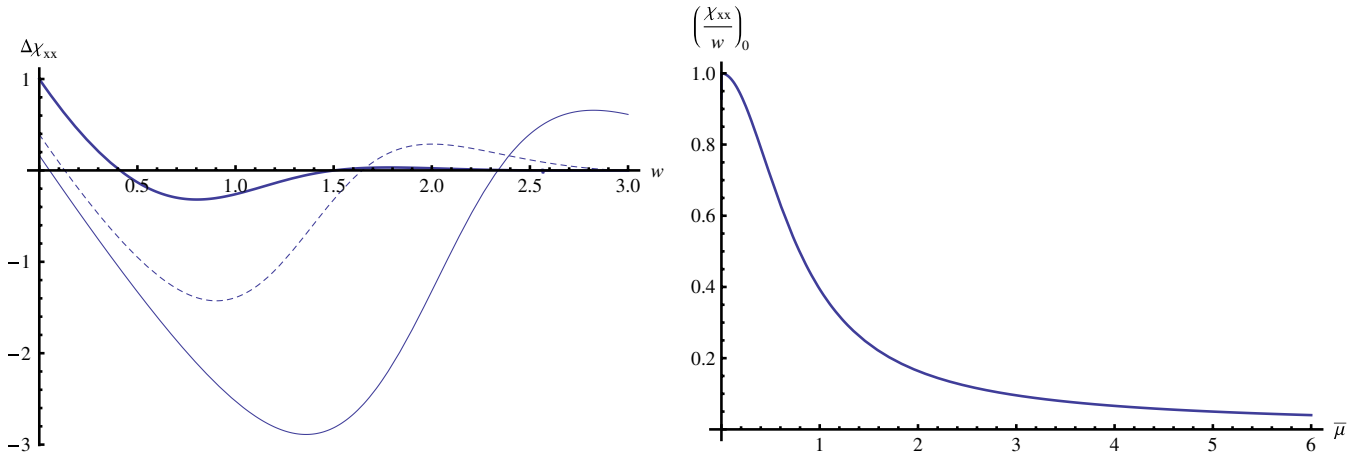

FIG. 2 (color online). $\Delta\chi_{xx}/\mathfrak{w}$, deviation of finite temperature thermal spectral function from the zero temperature spectral function, with $\bar{\mu} = 0$ (thick), 1 (dashed), 2. The normalization unit is $(2\pi T)^2 \frac{l}{2e^2}$. Right: The density dependence of DC conductivity with normalization constant $\frac{1}{2}\frac{l}{e^2}2\pi T$.

Yang-Mills plasma. It is interesting that for the tensor and vector mode the peak position is different. For the $\mathfrak{w} = 0$, χ_{xx} is zero so screening mass is zero. But for the finite $\mathfrak{w}$ there is the peak and the position is a function of both $\mathfrak{w}$ and $\bar{\mu}$. Because the diffusive nature affects the interactions inside the medium, the screening effect are more complicated. In fact, one can find the most notable effect of the density in Fig. 3: A peak appears in the spectral function which is absent at zero chemical potential. We attribute the origin of this effect to the appearance of the diffusion pole which was discovered in [13]. Since the residue of the pole is proportional to the charge we can expect that the new peak in spectral density is enhanced as charge increases. Indeed the numerical calculation confirms such expectations.

The hydrodynamic pole in G_{xx} appeared in Fig. 4 at

$$\mathfrak{w} \sim -i\frac{1 - a/2}{2(1 + a)}\mathfrak{q}^2. \tag{5.16}$$

The left figure shows that the hydrodynamic pole position is shifted from 0.0225 ($\mathfrak{q} = 0.3$) to 0.01 ($\mathfrak{q} = 0.2$). This comes from the density effect, when μ goes to zero the hydrodynamic pole in G_{xx} disappears, see Appendix C. This is the operator mixing result. The diffusion pole only appeared in $G_{xt,xt}$ or $G_{xz,xz}$ not $G_{x,x}$. The right figure shows that χ_{xx} reaches very rapidly to the zero temperature spectral function.

Figure 5 shows the real part of ac conductivity, $\mathrm{Re}\sigma(\mathfrak{w}) = \frac{\chi_{xx}(\mathfrak{w},\mathfrak{q}=0)}{i\mathfrak{w}}$ with the normalization unit $(2\pi T)^2\frac{l}{2g_5^2}$. By definition, $\mathrm{Im}\sigma = \frac{\mathrm{Re}G_{xx}}{w}$, $\mathrm{Re}\sigma = \frac{\mathrm{Im}G_{xx}}{w}$. The ac resistivity is defined as $\rho(\mathfrak{w}) = 1/\sigma(\mathfrak{w})$. For large $\mathfrak{w}$, the system has zero resistivity, which means that at any density charge carrying is almost perfect in high frequency.

The (xt, xt) component of spectral function χ_{xtxt} has the diffusion pole at $\mathfrak{w} = \mathfrak{q}^2/2$ [19]. The dispersion relation for diffusive channel $w = Dk^2/2$ gives us the diffusion constant $D = 1/2\pi T$ from the hydrodynamic analysis.

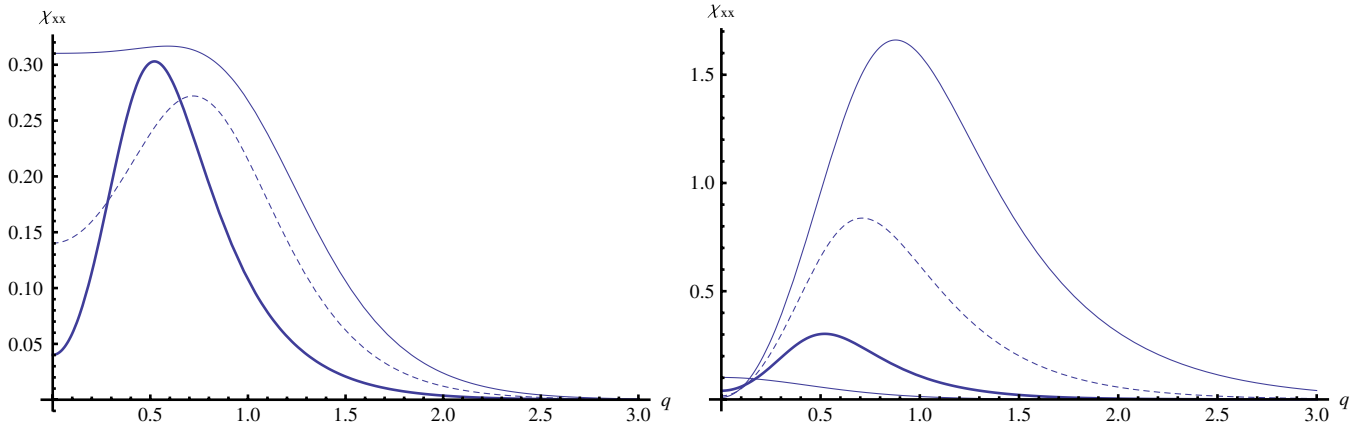

FIG. 3 (color online). The normalized thermal spectral function $\chi_{xx}(\mathfrak{q})$. Left: with $\bar{\mu} = 1$ and varying $\mathfrak{w} = 0.1$ (thick), 0.3 (dashed), 0.5 (thin); right $\mathfrak{w} = 0.1$ and varying $\bar{\mu} = 0$ (lowest thin line), 1 (thick), 2 (dashed), 3 (solid), with normalization unit $(2\pi T)^2\frac{l}{2g_5^2}$.

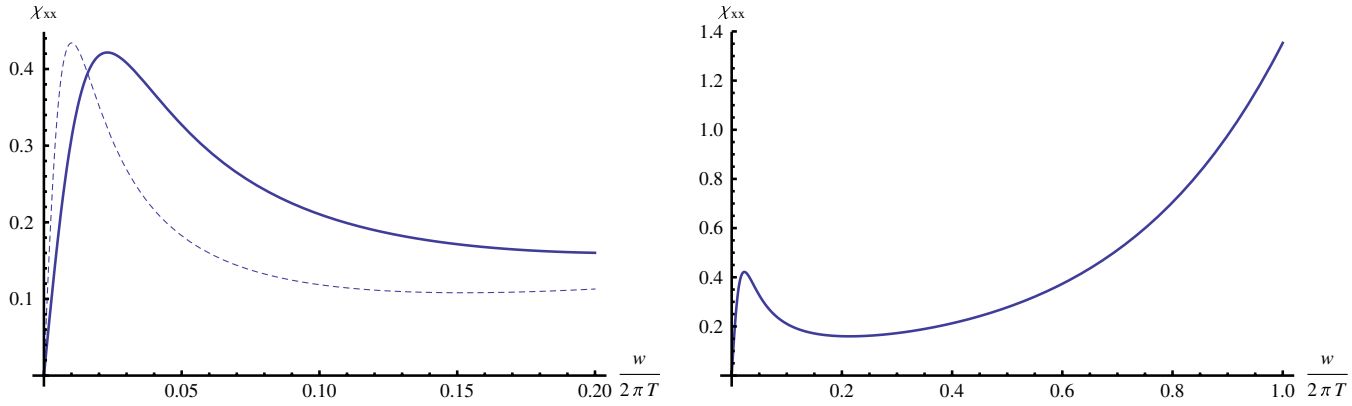

FIG. 4 (color online). $\Delta\chi_{xx}$ for various density, one with $a = 0.5$, $\mathfrak{q} = 0.3$ (thick), $a = 0.5$ $\mathfrak{q} = 0.2$ (dashed). The normalization unit is $(2\pi T)^2 \frac{l}{2e^2}$. Right: χ_{xx} ($a = 0.5$, $\mathfrak{q} = 0.3$) plotted in the range $\mathfrak{w} \in [0, 1]$.

The left part of Fig. 6 is with $\mathfrak{q} = 0.3$ for various values of $\bar{\mu}$: 0.5 (thick), 1 (dashed), 1.5 (thin). When the chemical potential grows, the strength of peak also grows but the position itself does not. The reason of this increase comes from the factor $\frac{1}{(1-a/2)^4}$ in front of the Green's function. When $\bar{\mu}$ increases the parameter a goes up so the overall factor $(1 - a/2)^{-4}$ increases rapidly. When the system reaches the extremal limit, $a = 2$, that factor diverges and our analysis is broken down. It should be computed separately for the zero temperature or for the extremal RN spectral function from finite temperature or nonextremal RN-AdS black hole.

In the right part of Fig. 6, the peak position is shifted when $\mathfrak{q}$ is moved. Again, the position is at $\mathfrak{w} = \mathfrak{q}^2/2$.

VI. PHOTOEMISSION RATE

In the heavy ion collision, the emitted photons are a good measure to see the medium effect. The photoemission rate of SYM plasma was calculated holographically for AdS Schwarzschild [16], for $D4/D8/\bar{D}8$ with finite chemical potential [17] and for $D3/D7$ with finite density [24]. We will focus on the photoemission rate for our gauge theory dual to the RN-AdS background here. Let Γ_γ be the number of photons emitted per unit volume. To leading order in electromagnetic coupling e,

$$d\Gamma_\gamma = \frac{d^3k}{(2\pi)^3}\frac{e^2}{2|\vec{k}|}\eta^{\mu\nu}C^<_{\mu\nu}(K)|_{w=k}$$
$$C^<_{\mu\nu}(K) = n_B(w)\chi_{\mu\nu}(K), \tag{6.1}$$

where $C^<_{\mu\nu}(K)$ is the Fourier transformed Wightman function which is related to the spectral function multiplied by Bose-Einstein distribution function $n_B(w)$. Convert the differential photoemission rate into the emission rate per unit volume as a function of ω,

$$\frac{d\Gamma_\gamma}{dk} = \frac{\alpha_{\mathrm{EM}}}{\pi}k\eta^{\mu\nu}C^<_{\mu\nu}(K)|_{\omega=k}. \tag{6.2}$$

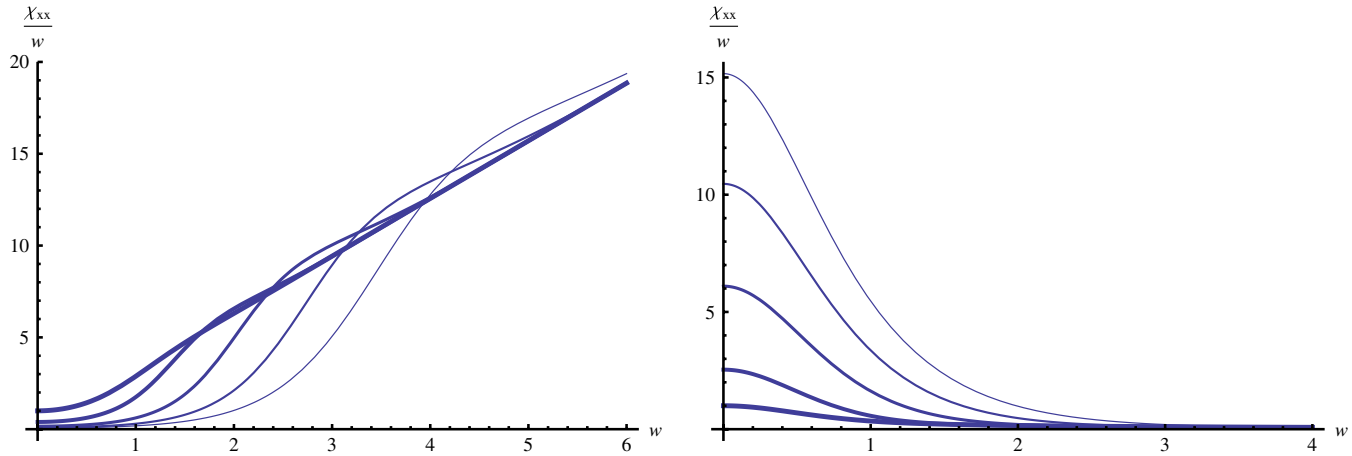

FIG. 5 (color online). Real part of AC conductivity of SYM plasma, $\chi_{xx}(\mathfrak{w}, \mathfrak{q} = 0)/\mathfrak{w}$ and the normalization unit is $(2\pi T)^2 \frac{l}{2g_5^2}$. Each line shows the result when $\bar{\mu} = 0$ (thick), 1, 2, 3, 4 (thin). Left: AC conductivity; right: AC resistivity as an inverse of the left one.

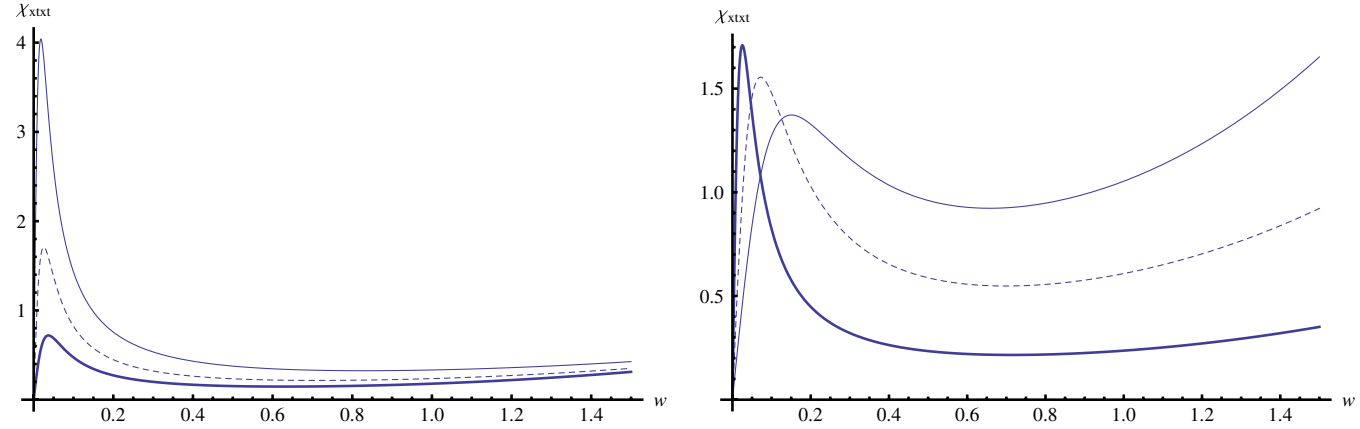

FIG. 6 (color online). The normalized thermal spectral function χ_{xtxt}. Left: with $\mathfrak{q} = 0.3$ and varying $\bar{\mu} = 0.5$ (thick), 1 (dashed), 1.5 (solid); right: with $\bar{\mu} = 1$ and varying $\mathfrak{q} = 0.3$ (thick), 0.5 (dashed), 0.7 (solid) with normalization unit $(2\pi T)^4 \frac{l^3}{16G_5^2}$.

In order to calculate the photoemission rate we need to know the longitudinal part of the spectral function. But for the case of lightlike momentum $\omega = k$, the trace of spectral function $\chi^\mu_\mu = \eta^{\mu\nu}\chi_{\mu\nu}$ is obtained only by Π^T. From Appendix A,

$$\eta^{\mu\nu}C^{\text{ret}}_{\mu\nu} = (d-2)\Pi^T + \Pi^L = 2\Pi^T + \Pi^L, \qquad (6.3)$$

where d is the dimension of the boundary field theory. For the lightlike momentum, the longitudinal correlator should be vanished because the projection operator diverges. The trace of spectral function is only given by $\Pi^T(w, |\vec{k}| = w)$.

In Fig. 7, the photoemission rate is presented as a function of $\mathfrak{w}$ compared with [16] which is given as the thickest line. The peak position is located at $\mathfrak{w}_{\text{max}} = 1.484\,79/(2\pi) = 0.2363$ and the maximum value is 0.015 67 with unit $\alpha_{\text{EM}}(N_c^2 - 1)T^3$. The left figure shows the photoemission rate for $\bar{\mu} = 0$ (thick), 1 (solid), 5 (dashed), 10 (thin) and the right shows the maximum value $\frac{d\Gamma_\gamma}{dk}(w = 0.2363)$ as a function of $\bar{\mu}$. Notice that the maximum value of the photoemission rate decreases until $\mathfrak{w}_c = 2.014$ which is the turning point. After passing $\bar{\mu}_c$ it increases. From the right figure, the photoemission rate is almost monotonic in large $\bar{\mu}$. Before the turning point $\bar{\mu}_c$, the maximum value is decreased and is also presented in the left one.

It means the thermal photon production rate is suppressed in the low chemical potential regime but in the high density regime, enhanced. It may reflect the fact that at high enough density thermal screening is enhanced. By comparing Ref. [16], at $\bar{\mu} = 0.1$ (from RHIC) the maximum value of the photoemission rate is decreased by 1% (0.015 669 5 to 0.015 515 8) which is almost negligible. The suppression of conductivity and the increase of thermal screening mass are presented in Figs. 2 and 3.

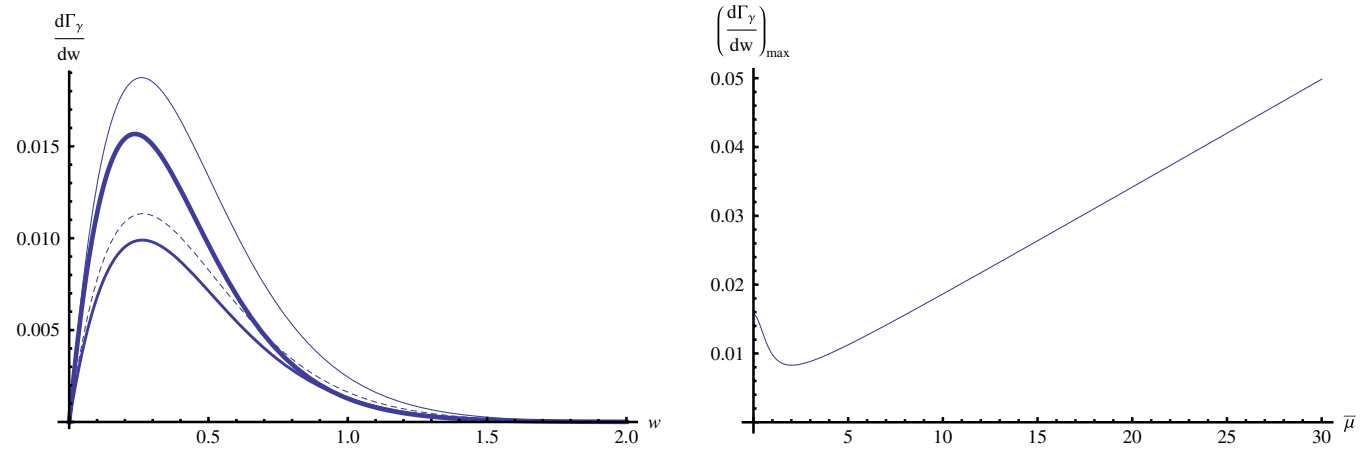

FIG. 7 (color online). The photoemission rate of SYM-electromagnetic (EM) plasma with normalization unit $\alpha_{\text{EM}}(N_c^2 - 1)T^3$. $d\Gamma_\gamma/dk$ with lightlike momenta. Left: varying $\bar{\mu} = 0$ (thick), 1 (solid), 5 (dashed), 10 (thin); right: the maximum value of the photoemission rate as a function of chemical potential $\bar{\mu}$.

When the U(1) chemical potential is very large, $a \sim 2$, the maximum value suddenly increases. Until $a = 1$, the maximum value is a slowly decreasing function of a, but after passing $a = 1$ it increases stiffly. But this sudden increase may be artificial, because if we express as the chemical potential this stiffness is not there. The frequency dependent spectral measure $\eta^{\mu\nu}\chi_{\mu\nu}/\mathfrak{w}$ for the lightlike momenta is in Fig. 8. The left part of Fig. 8 has three lines $\bar{\mu} = 0$ (thick), 5 (dashed), and 10 (thin).

Note that the spectral measure has a maximum at the point due to the hydrodynamic pole of G_{xx}:

$$G_{xx} \sim \frac{1}{w + iDk^2}, \qquad \text{where } D = \frac{b}{2(1+a)}. \tag{6.4}$$

The Green's function in the hydrodynamic limit, see Appendix C, presents the very essence of photoemission rate of dense supersymmetric Yang-Mills plasma:

$$\chi_{xx}^{\text{hydro}} = \frac{2l}{8e^2b^2}\left[\frac{3a}{1+a}\frac{Dk^2w}{D^2k^4+w^2} + \frac{2(1-a/2)^2}{(1+a)^2}bw\right]$$
$$= \frac{2l}{8e^2b^2}\left[\frac{3a}{1+a}\frac{D_a\tilde{\mathfrak{q}}^2\tilde{\mathfrak{w}}}{D_a^2\tilde{\mathfrak{q}}^4+\tilde{\mathfrak{w}}^2} + \frac{2(1-a/2)^3}{(1+a)^2}\tilde{\mathfrak{w}}\right],$$
$$D_a = \frac{1}{2(1+a)}. \tag{6.5}$$

Figure 9 shows the photoemission rate of the hydrodynamic approximated solution. The left part is almost the same as the full numerical solution but tails in large $\mathfrak{w}$ are different, and in the right part we plot $\mathfrak{w}^2/(e^{2\pi\mathfrak{w}}-1)$ as a

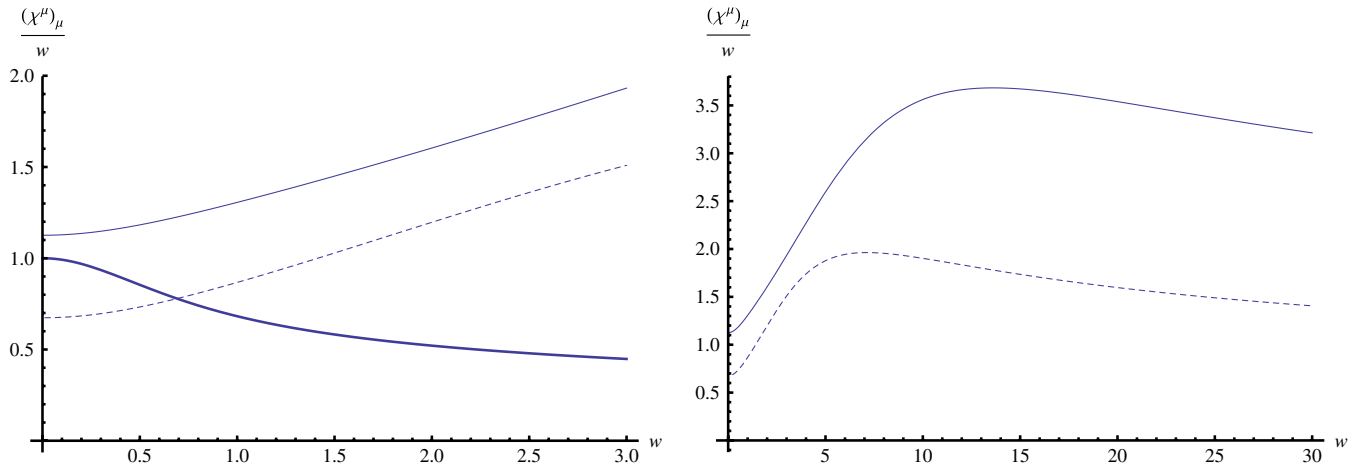

FIG. 8 (color online). The normalized trace of thermal spectral function $\chi^\mu_\mu/\mathfrak{w}$ with lightlike momenta. Left: varying $\bar{\mu} = 0$ (thick), 5 (dashed), 10 (thin); right: $\bar{\mu} = 5$ (dashed), 10 (thin) and the plotting range is from zero to 30 in $\mathfrak{w}$.

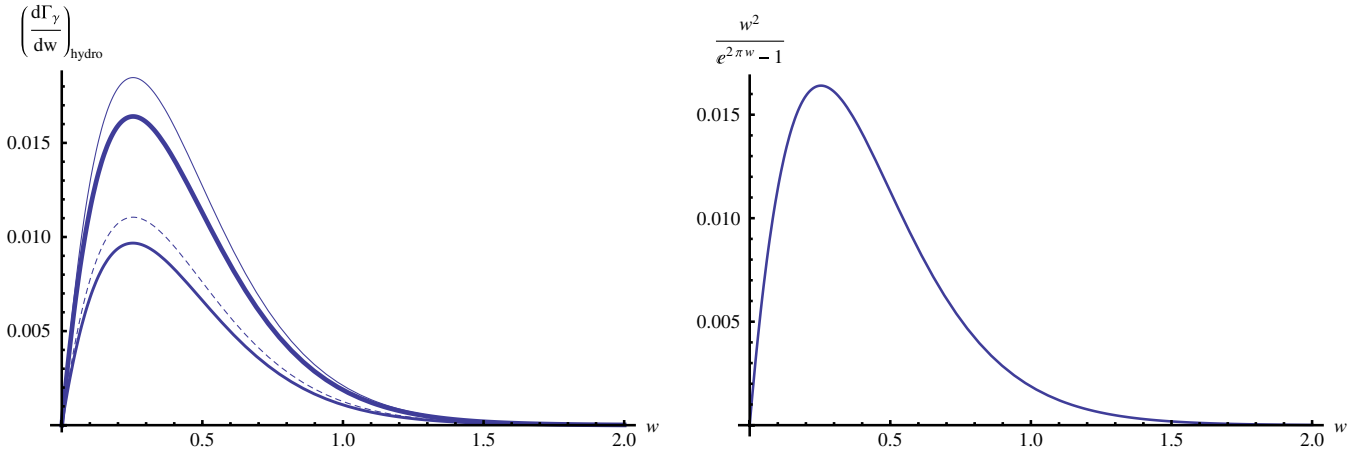

FIG. 9 (color online). The photoemission rate of hydrodynamic approximated spectral function with normalization unit $(2\pi T)^2\frac{l}{2g_5^2}$. $d\Gamma_\gamma/dk$ with lightlike momenta. Left: varying $\bar{\mu} = 0$ (thick), 1 (solid), 5 (dashed), 10 (thin); right: $\mathfrak{w}^2/(e^{2\pi\mathfrak{w}}-1)$ is plotted as a function of $\mathfrak{w}$.

function of $\mathfrak{w}$. The origin of the peak in the photoemission rate comes from the statistical factor and the change of height is the density effect. This density effect is almost described by a single function, Eq. (6.5).[6]

VII. CONCLUSION

We have solved the equation of motion for linearized gravitational and electromagnetic perturbations in the RN-AdS background to get the holographic spectral function. Because of the density effect, the gravitational and electromagnetic perturbations are coupled with each other so it is not easy to solve. By introducing a master variable, however, we can decouple these modes which makes the problem simpler. The problem might be handled without decoupling along the method discussed in [25].

The density effects of thermal spectral function have some interesting features. The boundary theory of RN AdS is believed supersymmetric Yang-Mills theory with finite U(1) charge density. The original SYM has no dimensionful parameter and does not admit any quantity like screening length, energy gap, diffusion constant, etc. In the finite temperature and density state, however, the plasma has a scale given by those.

One of the interesting features is the modification of the diffusive nature of thermal plasma. As we have seen in Fig. 2 the DC conductivity is decreasing in large $\bar{\mu}$. It is quite natural because in dense medium particles collide very frequently, so the charge carrying process should be suppressed.

The photoemission rate is a very important tool to probe the effects of thermal medium. Because the photon does not interact with other particles via strong interaction, it carries information of the early stage of collision. The holographic photoemission rate is greatly enhanced when $\bar{\mu}$ is very large. See Fig. 7. Note that information of spectral function over only a small window of $\mathfrak{w}$ is sufficient to describe the photoemission rate, because almost all of the contributions for photoemission rate come from the statistical factor $1/(e^{w/T}-1)$.

It would be interesting to see whether the U(1) axial anomaly [33–35] can affect the photoemission rate. We will report this issue in the near future.

ACKNOWLEDGMENTS

We give thanks to Yang Zhou and Antonio Amariti for the useful communications. This work was supported by the WCU project of Korean Ministry of Education, Science and Technology (R33-2008-000-10087- 0). This work is also supported by the Mid-career Researcher Program through NRF Grant No. 2010-0008456 and by the National Research Foundation of Korea (NRF) grant funded by the Korea government (MEST) (No. 2005-0049409).

APPENDIX A: THE INDEX STRUCTURE OF CORRELATION FUNCTIONS

The correlation functions of various operators have Lorentz index structure, and that has to satisfy some constraints, i.e. *CPT* invariance, Ward identity [19]. We will briefly review the index structure of our correlation functions for later convenience.

The definitions of retarded correlation function of conserved current and energy momentum tensor are

$$\begin{aligned} C_{\mu\nu}(x-y) &= -i\theta(x^0-y^0)\langle[J_\mu(x),J_\nu(y)]\rangle \\ G_{\mu\nu\alpha\beta}(x-y) &= -i\theta(x^0-y^0)\langle[T_{\mu\nu}(x),T_{\alpha\beta}(y)]\rangle. \end{aligned} \tag{A1}$$

In the equilibrium, *CPT* invariance told us that

$$C_{\mu\nu}=C_{\nu\mu}, \qquad G_{\mu\nu\alpha\beta}=G_{\alpha\beta\mu\nu}. \tag{A2}$$

In addition, correlation functions of the energy momentum tensor have the property inherited from the symmetry of the energy momentum tensor,

$$G_{\mu\nu\alpha\beta}=G_{\nu\mu\alpha\beta}=G_{\mu\nu\beta\alpha}. \tag{A3}$$

The Ward identity

$$k^\mu C_{\mu\nu}=0=k^\mu G_{\mu\nu\alpha\beta} \tag{A4}$$

and if the theory has scale invariance $T^\mu_\mu=0$,

$$\eta^{\mu\nu}G_{\mu\nu\alpha\beta}=0. \tag{A5}$$

From the Ward identity, the correlation functions are projected onto transverse spacetime of k^μ:

$$\begin{aligned} C_{\mu\nu} &= P_{\mu\nu}\Pi(K^2) \\ G_{\mu\nu\alpha\beta} &= P_{\mu\nu}P_{\alpha\beta}G_B(K^2)+H_{\mu\nu\alpha\beta}G_S(K^2), \end{aligned} \tag{A6}$$

where

$$\begin{aligned} P_{\mu\nu} &= \eta_{\mu\nu}-\frac{k_\mu k_\nu}{K^2} \\ H_{\mu\nu\alpha\beta} &= \frac{1}{2}(P_{\mu\alpha}P_{\nu\beta}+P_{\mu\beta}P_{\nu\alpha})-\frac{1}{D-1}P_{\mu\nu}P_{\alpha\beta}. \end{aligned} \tag{A7}$$

The field theory propagator is classified by boundary SO(2) rotation symmetry [19]. The propagator is decomposed as scalar, vector, tensor parts according to their transformation properties under SO(2). We assume that the wave is going along the z direction $K=(w,0,0,k)$ and the boundary coordinate is labeled by (t,x,y,z). The stress-energy tensor correlator $G_{\mu\nu\rho\sigma}$ is also decomposed into these categories. The conserved current, for our case R current, is projected as transverse and longitudinal parts,

$$C_{\mu\nu}=P^T_{\mu\nu}\Pi^T+P^L_{\mu\nu}\Pi^L, \tag{A8}$$

where $P^T_{\mu\nu}$, $P^L_{\mu\nu}$ is transverse and longitudinal projector which are mutually orthogonal

[6] But actually at large $\mathfrak{w}$, there are deviations between Figs. 7 and 9. Please note that it is an approximated solution.

$$P^T_{ij} = \delta_{ij} - \frac{k_i k_j}{\vec{k}^2},$$
$$P^T_{\mu 0} = P^T_{0\mu} = 0, \tag{A9}$$
$$P^L_{\mu\nu} = P_{\mu\nu} - P^T_{\mu\nu}.$$

Each component of the current-current correlator is

$$C_{xx}(K) = C_{yy}(K) = \Pi^T(K) \quad C_{tt}(K) = \frac{k^2}{w^2-k^2}\Pi^L,$$
$$C_{tz}(K) = \frac{-wk}{w^2-k^2}\Pi^L, \qquad C_{zz}(K) = \frac{w^2}{w^2-k^2}\Pi^L. \tag{A10}$$

For the stress-energy correlation function, the classification is slightly complicated:

$$\begin{aligned} G_{\mu\nu\alpha\beta}(K) = {} & (P^T_{\mu\nu}P^T_{\alpha\beta} + \tfrac{1}{2}(P^T_{\mu\nu}P^L_{\alpha\beta} + P^L_{\mu\nu}P^T_{\alpha\beta}))C_T \\ & + (P^T_{\mu\nu}P^T_{\alpha\beta} + \tfrac{1}{2}(P^T_{\mu\nu}P^L_{\alpha\beta} + P^L_{\mu\nu}P^T_{\alpha\beta}))C_L \\ & + S_{\mu\nu\alpha\beta}G_1 + Q_{\mu\nu\alpha\beta}G_2 + L_{\mu\nu\alpha\beta}G_3, \end{aligned} \tag{A11}$$

where

$$\begin{aligned} S_{\mu\nu\alpha\beta} &= \frac{1}{2}(P^T_{\mu\alpha}P^L_{\nu\beta} + P^T_{\mu\alpha}P^L_{\nu\beta} + P^T_{\mu\beta}P^L_{\nu\alpha} + P^L_{\mu\beta}P^T_{\nu\alpha}) \\ Q_{\mu\nu\alpha\beta} &= \frac{1}{D-1}\Big((D-2)P^L_{\mu\nu}P^L_{\alpha\beta} + \frac{1}{D-2}P^T_{\mu\nu}P^T_{\alpha\beta} \\ & \quad - (P^T_{\mu\nu}P^L_{\alpha\beta} + P^L_{\mu\nu}P^T_{\alpha\beta})\Big) \\ L_{\mu\nu\alpha\beta} &\equiv H_{\mu\nu\alpha\beta} - S_{\mu\nu\alpha\beta} - Q_{\mu\nu\alpha\beta}. \end{aligned} \tag{A12}$$

The transverse components of $G_{\mu\nu\alpha\beta}$ are

$$G_{txtx} = \frac{1}{2}\frac{k^2}{w^2-k^2}G_1, \qquad G_{txzx} = -\frac{1}{2}\frac{wk}{w^2-k^2}G_1,$$
$$G_{xzxz} = \frac{1}{2}\frac{w^2}{w^2-k^2}G_1, \qquad G_{xyxy} = \frac{1}{2}G_3 \tag{A13}$$

and longitudinal components of G are

$$\begin{aligned} G_{tttt} &= \frac{1}{3}\frac{k^4}{(w^2-k^2)^2}[2G_2 + 3C_L] \\ G_{tttz} &= -\frac{1}{3}\frac{wk^3}{(w^2-k^2)^2}[2G_2 + 3C_L] \\ G_{ttxx} &= \frac{1}{6}\frac{k^2}{w^2-k^2}[2G_2 - 3C_L - 3C_T]. \end{aligned} \tag{A14}$$

Note that if the theory has the scale invariance, C_L, C_T vanish.

APPENDIX B: LARGE $\mathfrak{w}$ SPECTRAL FUNCTIONS

In this section, we will calculate the spectral function analytically in the large frequency limit [18,21]. By using WKB methods, we can get the large frequency spectral function. This procedure is easily described by an example of the simple Schrödinger equation,

$$y''(x) + V(x)y(x) = 0. \tag{B1}$$

Transforming the wave function $y(x)$ into $\phi(x)$ by $y(x) = e^{i\phi(x)}$, we get

$$-(\phi')^2 + i\phi'' + V = 0. \tag{B2}$$

Assume that ϕ'' is subleading,

$$\phi' = \pm\sqrt{V}, \qquad |\phi''| \sim \frac{1}{2}\left|\frac{V'}{\sqrt{V}}\right| \ll |V| \tag{B3}$$

so the first order solution is

$$\phi = \pm\int\sqrt{V}dx. \tag{B4}$$

From Eq. (B2) we will obtain the second order solution by substituting the first order solution,

$$\begin{aligned} (\phi')^2 &\sim V \pm \frac{i}{2}\frac{V'}{\sqrt{V}} \\ \phi' &\sim \pm\sqrt{V} + \frac{i}{4}\frac{V'}{V} \\ \phi &= \pm\int\sqrt{V}dx + \frac{i}{4}\ln V, \end{aligned} \tag{B5}$$

so the WKB solution is

$$y(x) = \frac{1}{V^{1/4}}(e^{i\int\sqrt{V}dx} + e^{-i\int\sqrt{V}dx}). \tag{B6}$$

1. Tensor mode

For the tensor mode, the equation of motion for h^x_y is transformed into Schrödinger form by choosing $h^x_y(u) = X(u)\psi(u)$, where $X(u) = \sqrt{u/f(u)}$:

$$\begin{aligned} \psi'' + V(u)\psi &= 0, \\ V(u) &= -\frac{3}{4u^2} + \frac{1}{4}\frac{f'^2}{f^2} + \frac{f'}{2uf} - \frac{f''}{2f} \\ & \quad + \frac{(1-\frac{a}{2})^2}{uf^2}(\mathfrak{w}^2 - \mathfrak{q}^2 f). \end{aligned} \tag{B7}$$

This equation has two singular points at $u = 0$ and $u = 1$. From the WKB analysis, we get the two linearly independent solutions away from these singularities:

$$\begin{aligned} \psi_1 &\sim \frac{1}{\sqrt{p(u)}}\cos(S(u) + \phi_1), \\ \psi_2 &\sim \frac{1}{\sqrt{p(u)}}\sin(S(u) + \phi_2), \end{aligned} \tag{B8}$$

where

$$p(u) = \frac{1-\frac{a}{2}}{\sqrt{u}f}\sqrt{\mathfrak{w}^2 - \mathfrak{q}^2 f}, \qquad S(u) = \int_0^u p(z)dz. \tag{B9}$$

Near the boundary.—Near $u = 0$, the potential has the form

$$\psi'' + \left(-\frac{3}{4u^2} + \frac{Q^2}{u}\right)\psi = 0, \tag{B10}$$

where $Q^2 = (1 - \frac{a}{2})^2(\mathfrak{w}^2 - \mathfrak{q}^2)$. The general solution is

$$\psi = C_1\sqrt{u}J_2\left(\sqrt{4Q^2u}\right) + C_2\sqrt{u}Y_2\left(\sqrt{4Q^2u}\right). \tag{B11}$$

Bessel functions have the following asymptotic forms for large x ($x \gg |\alpha^2 - 1/4|$):

$$\begin{aligned} J_\alpha(x) &\sim \sqrt{\frac{2}{\pi x}}\cos\left(x - \frac{\alpha\pi}{2} - \frac{\pi}{4}\right), \\ Y_\alpha(x) &\sim \sqrt{\frac{2}{\pi x}}\sin\left(x - \frac{\alpha\pi}{2} - \frac{\pi}{4}\right). \end{aligned} \tag{B12}$$

We are considering large $\mathfrak{w}$, so asymptotic forms of Bessel are valid for our case,

$$\begin{aligned} \sqrt{u}J_2(\sqrt{4Q^2u}) &\sim \sqrt{u}\frac{1}{\sqrt{\pi}}\frac{1}{\sqrt{Q\sqrt{u}}}\cos\left(2Q\sqrt{u} - \frac{5\pi}{4}\right) \\ \sqrt{u}Y_2(\sqrt{4Q^2u}) &\sim \sqrt{u}\frac{1}{\sqrt{\pi}}\frac{1}{\sqrt{Q\sqrt{u}}}\sin\left(2Q\sqrt{u} - \frac{5\pi}{4}\right) \end{aligned} \tag{B13}$$

and these are well matched with our WKB solutions $p(u) \sim Q/\sqrt{u}$, $S(u) \sim 2Q\sqrt{u}$.

Near the horizon.—Near $u = 1$, the equation of motion is

$$\psi'' + \frac{1}{(1-u)^2}\frac{1 + \mathfrak{w}^2}{4} \tag{B14}$$

and the solution is

$$\psi = C_3(1-u)^{1/2(1-i\mathfrak{w})} + C_4(1-u)^{1/2(1+i\mathfrak{w})}. \tag{B15}$$

Near the horizon, the infalling wave is only physically relevant and this boundary condition is to choose C_4 as zero. We know the two asymptotic solutions and it should be matched at some point,

$$\begin{aligned} &\frac{1}{\sqrt{\pi p(u)}}\left[\cos\left(S(u) - \frac{5}{4\pi}\right) + i\sin\left(S(u) - \frac{5}{4\pi}\right)\right] \\ &\quad = C(1-u)^{1/2 - i\mathfrak{w}/2}, \end{aligned} \tag{B16}$$

then the solution $h_y^x(u) = X(u)\psi(u)$ is

$$iuJ_2\left(\sqrt{4Q^2u}\right) + uY_2\left(\sqrt{4Q^2u}\right) = C(1-u)^{-i\mathfrak{w}/2}. \tag{B17}$$

This is the solution for large $\mathfrak{w}$, $\mathfrak{q}$ with infalling boundary condition at the black hole horizon. We did not fix the coefficient C, yet it is determined by the condition $h_y^x(u = 0) = 1$. Near the boundary, Bessel functions have series solutions and

$$\begin{aligned} uJ_2\left(\sqrt{4Q^2u}\right) &\sim \frac{1}{2}Q^2u + O(u^3), \\ uY_2\left(\sqrt{4Q^2u}\right) &\sim -\frac{1}{\pi Q^2} + O(u). \end{aligned} \tag{B18}$$

Nothing is left, the solution is

$$h_y^x = -\pi Q^2\left(iuJ_2\left(\sqrt{4Q^2u}\right) + uY_2\left(\sqrt{4Q^2u}\right)\right), \tag{B19}$$

then the spectral function is

$$\begin{aligned} \chi_{xyxy}^{T=0} &= \frac{l^3}{16G_5^2}\left(\frac{2\pi T}{1 - a/2}\right)^4 \mathrm{Im}\left[\lim_{u\to 0}\frac{f(u)}{u}h_y^x h_y^{x\prime}\right] \\ &= \frac{l^3}{16G_5^2}(w^2 - k^2)^2\theta(w^2 - k^2), \end{aligned} \tag{B20}$$

where the theta function comes from the fact $\sqrt{Q^2}$ should be real.

2. Vector mode

For the vector mode, we have two master variables Ψ_+, Ψ_- and their equations of motions. These can be transformed into Schrödinger form by

$$\Psi_\pm = \frac{1}{\sqrt{f}}\psi_\pm. \tag{B21}$$

Then equations of motion are rewritten in terms of $\Psi_\pm$:

$$\begin{aligned} &\psi_\pm'' + V_\pm\psi_\pm = 0, \\ &V_\pm = \frac{\mathfrak{w}^2 - \mathfrak{q}^2 f}{uf^2}\left(1 - \frac{a}{2}\right)^2 + \frac{1}{4}\frac{f'^2}{f^2} \\ &\qquad - \frac{1}{f}\left(C_\pm - \frac{f'}{u} + \frac{f''}{2}\right). \end{aligned} \tag{B22}$$

The equation of motion for the master fields near the boundary is

$$\begin{aligned} 0 &= \psi'' + \frac{(\mathfrak{w}^2 - \mathfrak{q}^2)(1 - a/2)^2}{u}\psi \equiv \psi'' + \frac{Q^2}{u}\psi \\ \psi &\sim C_1\sqrt{u}J_1\left(2\sqrt{Q^2u}\right) + C_2\sqrt{u}Y_1\left(2\sqrt{Q^2u}\right). \end{aligned} \tag{B23}$$

Near the horizon,

$$\begin{aligned} 0 &= \psi'' + \frac{1 + w^2}{4(1-u^2)}\psi \\ \psi &\sim C_3(1-u)^{1/2 - i\mathfrak{w}/2} + C_4(1-u)^{1/2 + i\mathfrak{w}/2}. \end{aligned} \tag{B24}$$

For large Q^2, two WKB solutions are

$$\begin{aligned} \psi_1 &\sim \frac{1}{\sqrt{\pi p(u)}}\cos(S(u) + \phi_1), \\ \psi_2 &\sim \frac{1}{\sqrt{\pi p(u)}}\sin(S(u) + \phi_2), \end{aligned} \tag{B25}$$

where

$$p(u)=\frac{1-\frac{a}{2}}{\sqrt{u}f}\sqrt{\mathfrak{w}^2-\mathfrak{q}^2 f},\qquad S(u)=\int_0^u p(z)dz. \tag{B26}$$

This WKB solutions should be matched near boundary solutions

$$\begin{aligned}2\sqrt{u}J_1(2\sqrt{Q^2u})&\sim\sqrt{u}\sqrt{\frac{1}{\pi\sqrt{Q^2u}}}\cos\left(2\sqrt{Q^2u}-\frac{3\pi}{4}\right)\\ 2\sqrt{u}Y_1(2\sqrt{Q^2u})&\sim\sqrt{u}\sqrt{\frac{1}{\pi\sqrt{Q^2u}}}\sin\left(2\sqrt{Q^2u}-\frac{3\pi}{4}\right)\end{aligned} \tag{B27}$$

and physically relevant boundary condition at horizon, infalling condition $C_4=0$,

$$\begin{aligned}\Psi=\frac{\psi}{\sqrt{f}}&=2\sqrt{u}C\left(iJ_1\left(2\sqrt{Q^2u}\right)+Y_1\left(2\sqrt{Q^2u}\right)\right)\\ &=-\pi Q\sqrt{u}\left(iJ_1\left(2\sqrt{Q^2u}\right)+Y_1\left(2\sqrt{Q^2u}\right)\right)\end{aligned} \tag{B28}$$

and by the normalization condition, $\Psi(u=0)=1$, the coefficient $C=-\pi Q/2$. Then the spectral function for vector mode is given as

$$\begin{aligned}\chi_{xx}^{T=0}&=\frac{l}{4e^2b^2}\,\mathrm{Im}\frac{C_+\hat{\Pi}_+^{T=0}-C_-\hat{\Pi}_-^{T=0}}{C_+-C_-}=\frac{l}{4e^2b^2}\pi Q^2\\ &=\frac{l}{4e^2}(2\pi T)^2\pi(\mathfrak{w}^2-\mathfrak{q}^2)\theta(w^2-k^2).\end{aligned} \tag{B29}$$

3. Lightlike momenta

For the lightlike momenta, $w=k$, the equation of motion is simplified [18] by

$$\begin{aligned}&\psi_\pm''+(\tilde{\mathfrak{w}}^2H+G_\pm)\psi_\pm=0,\qquad \text{where } H=\frac{1-f}{uf^2},\\ &G_\pm=\frac{1}{4}\frac{f'^2}{f^2}-\frac{1}{f}\left(C_\pm-\frac{f'}{u}+\frac{f''}{2}\right).\end{aligned} \tag{B30}$$

Near the black hole horizon the solution should be infalling, $(1-u)^{-i(\mathfrak{w}/2)}$. The analytic solution for the equation is not known but we just consider the large $\mathfrak{w}$ limit only to compute asymptotic behavior of spectral function. For large $\mathfrak{w}$, the leading term is $\tilde{\mathfrak{w}}^2$ and we assume the change of the wave function in the domain $u\in(0,1)$ is not large.

For the large $\mathfrak{w}$ limit the first term in Eq. (B30) is dominant. Introducing a new variable ζ,

$$\zeta=\left[\frac{3}{2}\int_0^u\sqrt{-H(x)}dx\right]^{2/3}, \tag{B31}$$

the wave function is reexpressed as

$$\begin{aligned}&\psi_\pm=\left(\frac{d\zeta}{du}\right)^{-1/2}\qquad W=\left(\frac{-H}{\zeta}\right)^{-1/4}W\\ &0=\frac{d^2W}{d\zeta^2}-(\tilde{\mathfrak{w}}^2\zeta+\gamma)W,\\ &\qquad\text{where }\gamma=\frac{5}{16\zeta^2}+\left(\frac{4HH''-5H'^2}{16H^3}+\frac{G}{H}\right)\zeta,\end{aligned} \tag{B32}$$

where the prime denotes derivative with respect to u, then the solution $\psi_\pm$ is Airy function,

$$\begin{aligned}\Psi_\pm=\frac{1}{\sqrt{f}}\psi_\pm&=\frac{1}{\sqrt{f}}\left(\frac{\zeta}{-H}\right)^{1/4}Ai(\tilde{\mathfrak{w}}^{2/3}\zeta(u))+\cdots\\ &=\left(\frac{u\zeta}{f-1}\right)^{1/4}Ai(\tilde{\mathfrak{w}}^{2/3}\zeta(u))+\cdots.\end{aligned} \tag{B33}$$

Two point functions for master variables are given as

$$\Pi_\pm=\lim_{u\to0}\frac{\Psi_\pm'}{\Psi_\pm}=\lim_{u\to0}\left(\frac{1}{4}\partial_u\ln\left(\frac{u\zeta}{1-f}\right)+\frac{\partial_u Ai(\tilde{\mathfrak{w}}^{2/3}\zeta(u))}{Ai(\tilde{\mathfrak{w}}^{2/3}\zeta(u))}\right) \tag{B34}$$

since $f-1=-u^2(1+a-au)$, and

$$\lim_{u\to0}\zeta=\frac{(1+a)^{1/3}(i(4+3a+\sqrt{1+a}(4+a)))^{2/3}}{(\sqrt{1+a}+1)^2}u+\cdots. \tag{B35}$$

The second term in the equation is

$$\begin{aligned}\lim_{u\to0}\partial_u\ln\left(\frac{u\zeta}{1-f}\right)&=\lim_{u\to0}\partial_u\ln\left(\frac{\zeta}{u(1+a-au)}\right)\\ &\sim\lim_{u\to0}\partial_u\ln\left(\frac{1}{(1+a)}\right)=0.\end{aligned} \tag{B36}$$

So the two point function is

$$\begin{aligned}\Pi_\pm&=-e^{i\pi/3}\frac{3^{1/3}(1+a)^{1/3}(4+3a+\sqrt{1+a}(4+a))^{2/3}}{(1+\sqrt{1+a})^2}\frac{\Gamma(\frac{2}{3})}{\Gamma(\frac{1}{3})}\tilde{\mathfrak{w}}^{2/3}\\ \mathrm{Im}\Pi_\pm&=\frac{3^{5/6}(1+a)^{1/3}(4+3a+\sqrt{1+a}(4+a))^{2/3}}{2(1+\sqrt{1+a})^2}\frac{\Gamma(2/3)}{\Gamma(1/3)}\tilde{\mathfrak{w}}^{2/3}\\ \chi_\mu^\mu&=\frac{l}{4e^2}\frac{(2\pi T)^2}{(1-a/2)^{4/3}}\frac{3^{5/6}(1+a)^{1/3}(4+3a+\sqrt{1+a}(4+a))^{2/3}}{(1+\sqrt{1+a})^2}\frac{\Gamma(2/3)}{\Gamma(1/3)}\mathfrak{w}^{2/3}.\end{aligned} \tag{B37}$$

In Fig. 10, we compare the numerically computed thermal spectral function for $\bar{\mu}=5$ with the zero temperature spectral function.

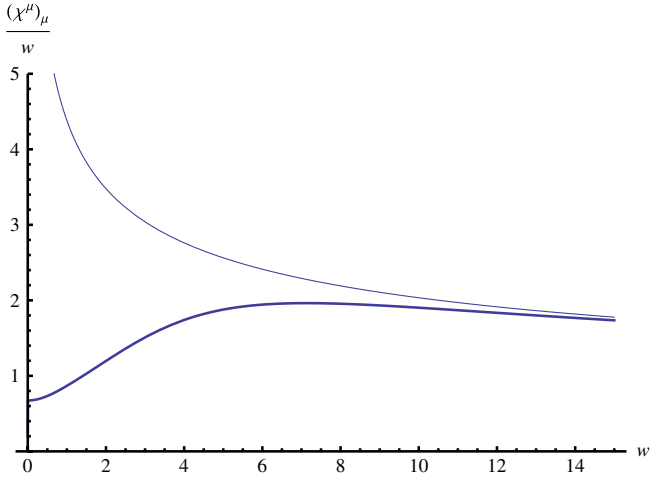

FIG. 10 (color online). The normalized trace of thermal spectral function $\chi^\mu_\mu/\mathfrak{w}$ with light like momenta. The thick line is for $\bar{\mu} = 5$ and the thin line is for the zero temperature case.

APPENDIX C: SMALL $\mathfrak{w}$ SPECTRAL FUNCTIONS

To check the consistency of numerical calculation, it is good to compare both the large frequency and the low frequency result with numerical computation. In the low frequency limit, authors [13] did the hydrodynamic analysis and it also gives us the low frequency spectral function. For the tensor mode,

$$\lim_{\mathfrak{w}\to 0} \mathrm{Im} G_{xyxy} = \frac{l^3}{16G_5^2}\frac{(2\pi T)^4}{(1-a/2)^3}\mathfrak{w}$$
$$\lim_{\mathfrak{w}\to 0} \frac{\chi_{xyxy}}{\mathfrak{w}} = \frac{l^3}{16G_5^2}\frac{(2\pi T)^4}{(1-a/2)^3}. \tag{C1}$$

For the vector mode G_{xx},

$$\lim_{\mathfrak{w}\to 0} \mathrm{Im} G_{xx} = \frac{l}{4e^2}\left[\frac{3a}{(1+a)b^2}\frac{D k^2 \mathfrak{w}}{D^2k^4 + w^2} + \frac{2(1-a/2)^2}{(1+a)^2 b} w\right]$$
$$\lim_{\mathfrak{w}\to 0} \frac{\chi_{xx}}{\mathfrak{w}} = \frac{l}{4e^2}\frac{(2\pi T)^2}{(1-a/2)^2}\left[\frac{3a}{1+a}\frac{D\mathfrak{q}k}{D^2\mathfrak{q}^2k^2 + \mathfrak{w}^2} + 2\frac{(1-a/2)^3}{(1+a)^2}\right]$$
$$\lim_{\mathfrak{w}\to 0}\lim_{\mathfrak{q}\to 0} \frac{\chi_{xx}}{\mathfrak{w}} = (2\pi T)^2 \frac{l}{4e^2}\frac{2(1-a/2)}{(1+a)^2}, \tag{C2}$$

where $D = \frac{b}{2(1+a)}$. For the G_{xtxt} in small $\mathfrak{w}$, $\mathfrak{q}$ limit,

$$\mathrm{Im} G_{xtxt} = \frac{l^3}{16G_5^2}\frac{1}{b^3}\frac{w k^2}{D^2k^4 + w^2}$$
$$\chi_{xtxt} = \frac{l^3}{16G_5^2}\frac{(2\pi T)^4}{(1-a/2)^3}\frac{\mathfrak{w}\mathfrak{q}^2}{D^2\mathfrak{q}^2k^2 + \mathfrak{w}^2}. \tag{C3}$$

APPENDIX D: BOUNDARY ACTION

In this section, we will briefly mention how to get rid of the divergences from the on-shell gravity action. The gauge/gravity correspondence tells us that the generating functional of the gauge theory is identified with the generating functional of the AdS gravity. As we have seen in Sec. 2.II, from the generating functional we get the two point functions of the boundary theory $G^{\mathrm{ret}}_{\mu\nu}$ or $G^{\mathrm{ret}}_{\alpha\beta,\mu\nu}$. The generating functional has some divergences which could be safely removed by adding counterterms, so-called holographic renormalization. At the boundary $u = 0$, there are two types of divergences $1/u$ and $\log u$.

The original action, Eq. (3.1), has Einstein-Hilbert, Maxwell, and Gibbons-Hawking terms and to remove the divergences we need the following counterterm [27] for the regularized action at the boundary:

$$S_{\mathrm{ct}} = S_{\mathrm{ct,gravity}} + S_{\mathrm{ct,gauge}} = \frac{1}{16G_5^2}\int d^4x\sqrt{-g^{(4)}}\left(\frac{3}{l} - \frac{l}{4}K\right) + \frac{l}{8e^2}\log u \int d^4x\sqrt{-g^{(4)}}\mathcal{F}_{mn}\mathcal{F}^{mn}, \tag{D1}$$

where K is the curvature on the boundary. $S_{\mathrm{ct,gravity}}$ is given in [36]. On the other hand, $S_{\mathrm{ct,gauge}}$ is obtained to cancel the logarithmic divergence coming from gauge field fluctuations. The boundary action for the perturbation in quadratic order derived from (3.1) is

$$S^{(0)} = \frac{l^3}{32b^4G_5^2}\int\frac{d^2k}{(2\pi)^2}\frac{1}{u^2}\left[\frac{uf'}{f}(h^x_t)^2 + h^x_t(h^x_t - 3uh^{x\prime}_t) - fh^x_z(h^x_z - 3uh^{x\prime}_z) + 3aB_x(h^x_t - fB'_x)\right]. \tag{D2}$$

The Gibbons-Hawking term and the counterterm (D1) are

$$S^{(0)}_{\mathrm{GH}} = \frac{l^3}{32b^4G_5^2}\frac{1}{u^2}\int\frac{d^2k}{(2\pi)^2}\left\{-\frac{uf'}{f}(h^i_t)^2 - 4(h^i_t)^2 - uf'(h^i_z)^2 + 4uh^i_t h^{i\prime}_t + 4f((h^i_z)^2 - uh^i_z(h^i_z)')\right\}, \tag{D3}$$

$$S^{(0)}_{\mathrm{ct}} = \frac{3l^3}{32b^4G_5^2}\frac{1}{u^2\sqrt{f}}\int\frac{d^2k}{(2\pi)^2}((h^i_t)^2 - f(h^i_z)^2 + ab^2k^2u^2f(u)\log u(B^2_x)). \tag{D4}$$

Then, the regularized boundary action is given as

$$S_{\mathrm{bdry}} = \lim_{u\to 0}(S^{(0)} + S^{(0)}_{\mathrm{GH}} + S^{(0)}_{\mathrm{ct}}) = \lim_{u\to 0}\frac{l^3}{32b^4G_5^2}\int\frac{d^2k}{(2\pi)^2}\left\{\frac{1}{u}(h^x_t(-k)h^{x\prime}_t(k) - h^x_z(-k)h^{x\prime}_z(k)) + 3aB_x(-k)(h^x_t(k) - B'_x(k)) + 3ab^2k^2\log u(B_x(-k)B_x(k))\right\}. \tag{D5}$$

[1] J. M. Maldacena, Adv. Theor. Math. Phys. **2**, 231 (1998); Int. J. Theor. Phys. **38**, 1113 (1999).
[2] S. S. Gubser, I. R. Klebanov, and A. M. Polyakov, Phys. Lett. B **428**, 105 (1998).
[3] E. Witten, Adv. Theor. Math. Phys. **2**, 253 (1998).
[4] G. Policastro, D. T. Son, and A. O. Starinets, Phys. Rev. Lett. **87**, 081601 (2001).
[5] P. Kovtun, D. T. Son, and A. O. Starinets, Phys. Rev. Lett. **94**, 111601 (2005).
[6] D. T. Son and A. O. Starinets, J. High Energy Phys. 09 (2002) 042.
[7] G. Policastro, D. T. Son, and A. O. Starinets, J. High Energy Phys. 09 (2002) 043.
[8] N. Armesto *et al.*, J. Phys. G **35**, 054001 (2008).
[9] P. Staszel (CBM Collaboration), Acta Phys. Pol. B **41**, 341 (2010).
[10] D. T. Son and A. O. Starinets, J. High Energy Phys. 03 (2006) 052.
[11] J. Mas, J. High Energy Phys. 03 (2006) 016.
[12] K. Maeda, M. Natsuume, and T. Okamura, Phys. Rev. D **73**, 066013 (2006).
[13] X. H. Ge, Y. Matsuo, F. W. Shu, S. J. Sin, and T. Tsukioka, Prog. Theor. Phys. **120**, 833 (2008).
[14] Y. Matsuo, S. J. Sin, S. Takeuchi, T. Tsukioka, and C. M. Yoo, Nucl. Phys. **B820**, 593 (2009).
[15] K. Jo, B. H. Lee, C. Park, and S. J. Sin, J. High Energy Phys. 06 (2010) 022.
[16] S. Caron-Huot, P. Kovtun, G. D. Moore, A. Starinets, and L. G. Yaffe, J. High Energy Phys. 12 (2006) 015.
[17] A. Parnachev and D. A. Sahakyan, Nucl. Phys. **B768**, 177 (2007).
[18] A. Nata Atmaja and K. Schalm, J. High Energy Phys. 08 (2010) 124.
[19] P. K. Kovtun and A. O. Starinets, Phys. Rev. D **72**, 086009 (2005).
[20] P. Kovtun and A. Starinets, Phys. Rev. Lett. **96**, 131601 (2006).
[21] D. Teaney, Phys. Rev. D **74**, 045025 (2006).
[22] R. C. Myers, A. O. Starinets, and R. M. Thomson, J. High Energy Phys. 11 (2007) 091.
[23] J. Erdmenger, M. Kaminski, and F. Rust, Phys. Rev. D **77**, 046005 (2008).
[24] J. Mas, J. P. Shock, J. Tarrio, and D. Zoakos, J. High Energy Phys. 09 (2008) 009.
[25] M. Kaminski, K. Landsteiner, J. Mas, J. P. Shock, and J. Tarrio, J. High Energy Phys. 02 (2010) 021.
[26] D. Mateos and L. Patino, J. High Energy Phys. 11 (2007) 025.
[27] K. Skenderis, Classical Quantum Gravity **19**, 5849 (2002).
[28] S. J. Sin, J. High Energy Phys. 10 (2007) 078.
[29] B. de Wit, G. Lopes Cardoso, D. Lust, T. Mohaupt, and S. J. Rey, Nucl. Phys. **B481**, 353 (1996).
[30] M. Edalati, J. I. Jottar, and R. G. Leigh, J. High Energy Phys. 04 (2010) 075.
[31] S. J. Sin and I. Zahed, Phys. Lett. B **608**, 265 (2005).
[32] C. P. Herzog, A. Karch, P. Kovtun, C. Kozcaz, and L. G. Yaffe, J. High Energy Phys. 07 (2006) 013.
[33] B. Sahoo and H. U. Yee, Phys. Lett. B **689**, 206 (2010).
[34] H. U. Yee, J. High Energy Phys. 11 (2009) 085.
[35] Y. Matsuo, S. J. Sin, S. Takeuchi, and T. Tsukioka, J. High Energy Phys. 04 (2010) 071.
[36] V. Balasubramanian and P. Kraus, Commun. Math. Phys. **208**, 413 (1999).